Supplementary Information

Preparation and structural adjustment of vanadium oxide nanotube as cathode material for PIBs with improved performance

AUTHOR NAMES. *Yuan Xie[a], Jia Wen[a], Junyuan Huang[a], Rong Jiang[a], Longjun Dai[a], Yang Ren[a], Zhu Liu[a, b], Xiaowei Zhou[a] , **

AUTHOR ADDRESS.

[a] Department of Physics, School of Physics and Astronomy, Yunnan University, Kunming, 650504, China.

[b] Yunnan Key Laboratory of Micro/Nano-Materials and Technology, School of Materials and Energy, Yunnan University, Kunming, 650504, China.

* Corresponding author's e-mail: zhouxiaowei@ynu.edu.cn (X.W. Zhou)

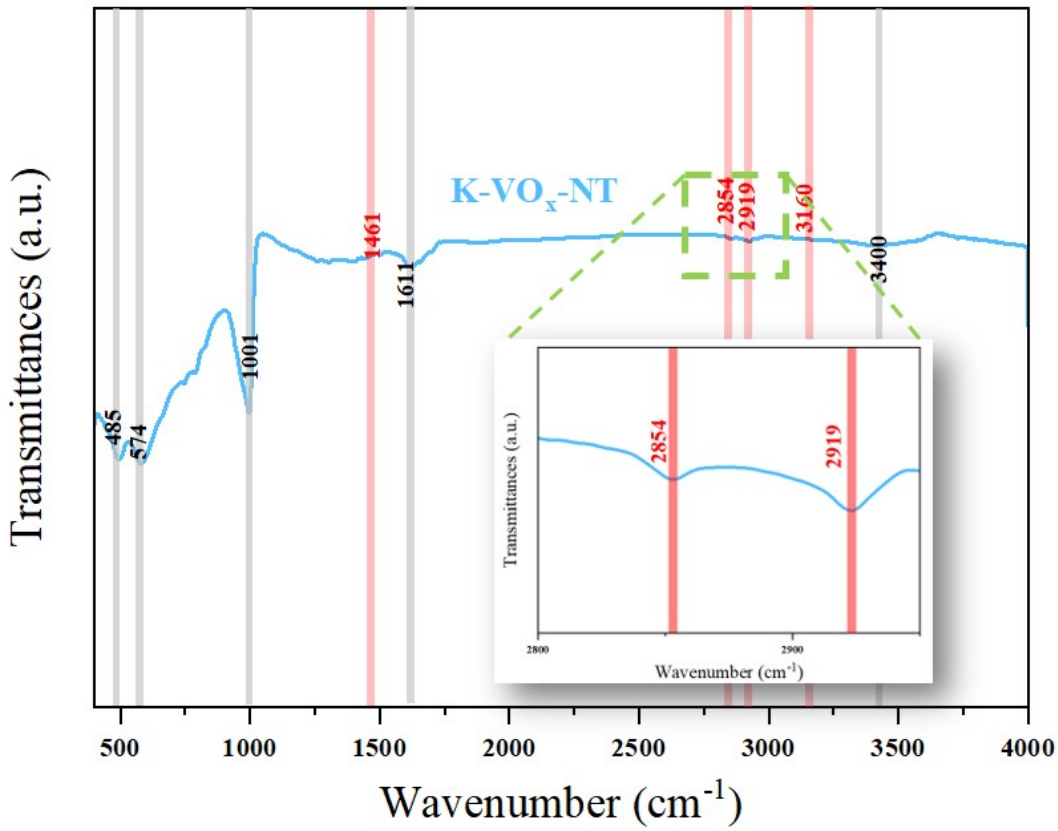

Figure S1. FTIR spectrum of K-VO_x-NT with an enlarged inset highlighting specific vibrational modes.

Fig. S1 shows FTIR spectrum of K-VO_x-NT sample. The inset provides a magnified view of two typical absorption peaks located at 2854 and 2919 cm^{-1}, which correspond to different stretching and bending vibration modes of C-H bonds in dodecylamine. It is evident that although the K^+ exchange process can effectively remove the organic template ($C_{12}H_{25}NH_3^+$) between VO_x layers, a small amount of organic template is still preserved. This residual organic template is one of the reasons for clear detection of carbon signals in the subsequent EDX mappings of K-VO_x-NT.

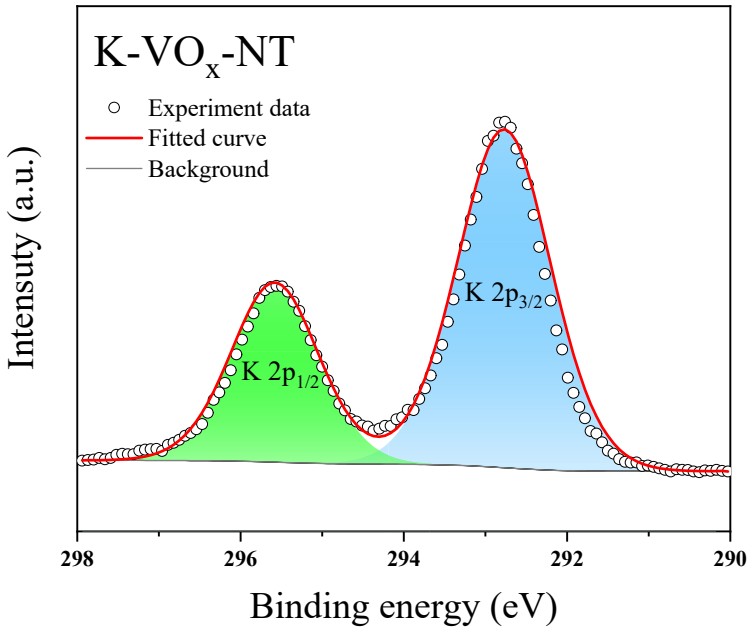

Figure S2. XPS fine survey spectrum of K_{2p} for K-VO_x-NT.

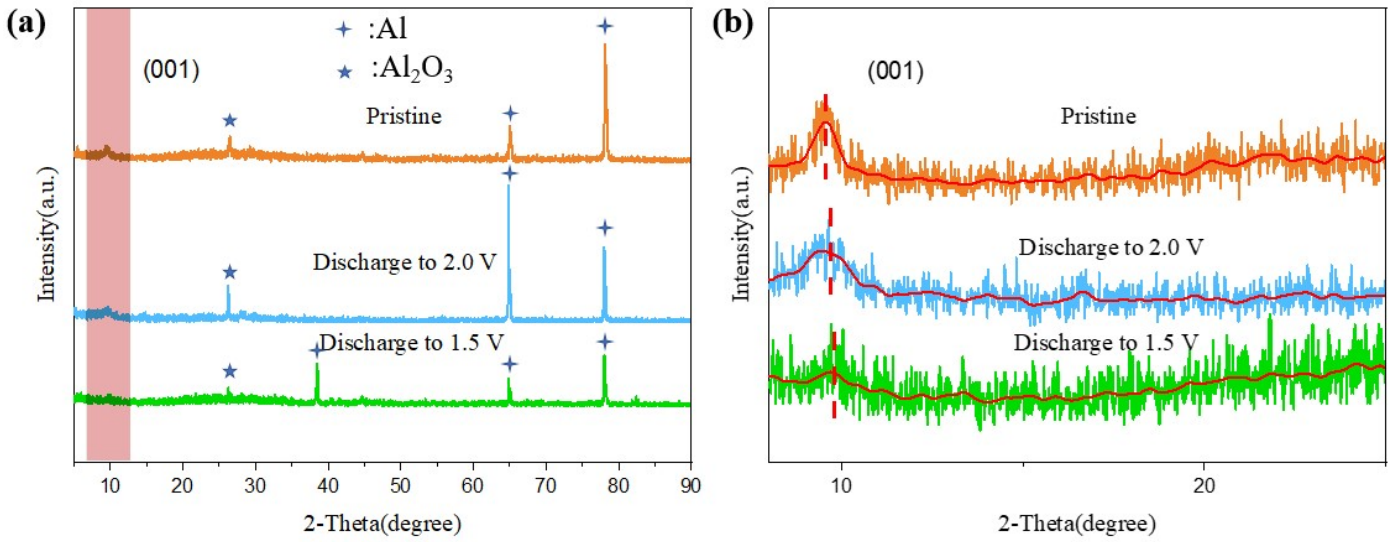

Figure S3. Ex-situ XRD patterns (a) of K-VO_x-NT at pristine, discharge to 2.0 V and 1.5 V states; Enlarged view (b) of (001) peaks in corresponding ex-situ XRD patterns.

To further investigate K^+ storage mechanism of K-VO_x-NT during the discharge process, ex-situ XRD tests at pristine, discharge to 2.0 V and 1.5 V states were performed as illustrated in Fig. S2 (a). The (001) peak for K-VO_x-NT exhibits a slight shift during the discharge process, moving from 9.6° in the pristine state to 9.9° at a discharge state of 1.5 V. The enlarged image for this shift was displayed in Fig. S2 (b). This shift corresponds to a minor contraction of interlayer spacing, which can be attributed to the enhanced interaction between intercalated K^+ and negatively charged VO_x layers as well as the reduced electrostatic repulsion between O^{2-} in adjacent layers [1]. However, owing to the very small shift of only 0.3°, the change in (001) interlayer spacing is hard to be detected by TEM.

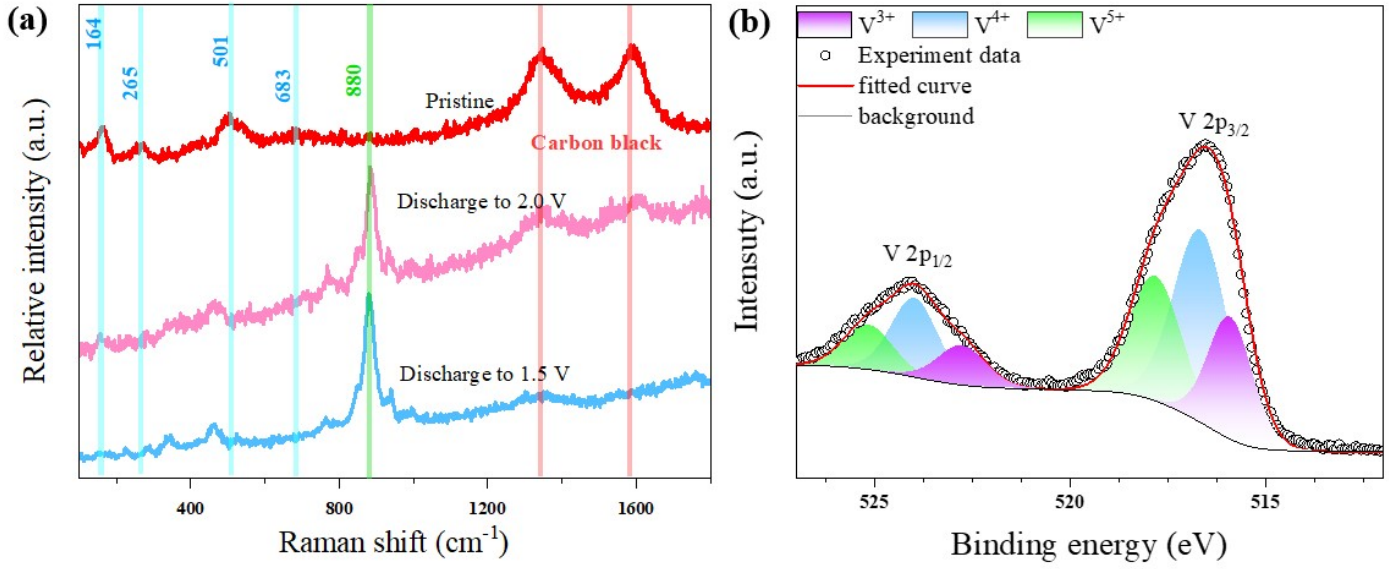

Figure S4. Ex-situ Raman spectra (a) of K-VO_x-NT at pristine, discharge to 2.0 V and 1.5 V states; (b) XPS fine survey spectra of V_{2p} for K-VO_x-NT under the fully

discharged (1.5 V) state.

Raman spectra were collected at pristine, discharge to 2.0 V and 1.5 V states for K-VO_x-NT cathode in Fig. S3 (a). A distinct peak appears at 880 cm^{-1} after discharging to 2.0 and 1.5 V, which can be attributed to the stretching vibration of V^{4+}=O bond [2]. It indicates that V^{5+} in pristine K-VO_x-NT would gradually transform into V^{4+}. Fig. S3(b) shows V2p fine spectrum of K-VO_x-NT in the fully discharged state. In comparison to V2p fine spectrum in the fully charged state as shown in Fig. 5 (d), the appearance of V^{3+} peak is observed, accounting for 24.1% of total V elements based on the peak area. Additionally, the V^{4+}/V^{5+} ratio increases significantly (from 66.2 % in the fully charged state to 159.0 % in the fully discharged state). This indicates that a portion of V^{4+} and V^{5+} is reduced to V^{3+} and V^{4+} upon K^+ intercalation, respectively. This is consistent with the ex-situ Raman results.

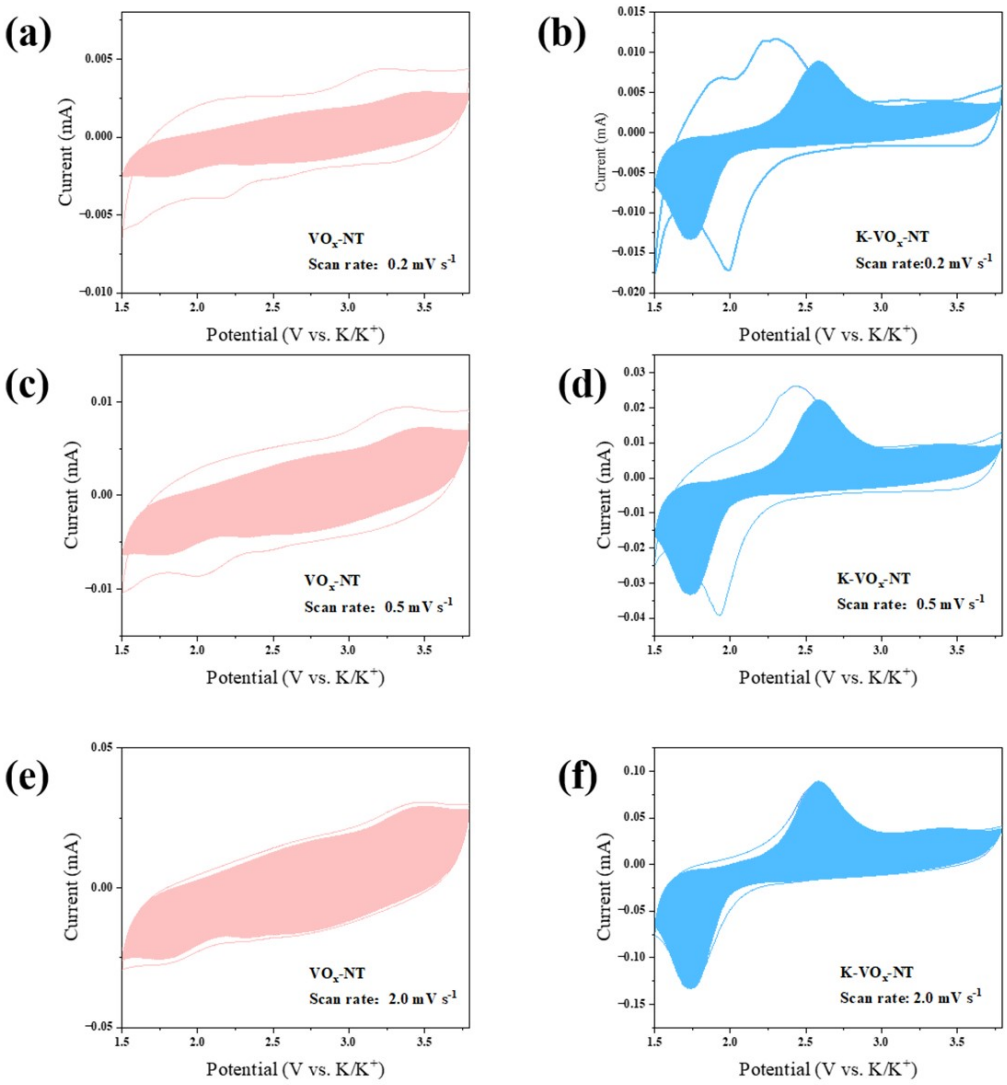

Figure S5. Pseudocapacitive contributions (shadow areas) from surface-induced process under representative CV test at 0.2, 0.5 and 2.0 mV s^{-1} for VO_x-NT (a, c, e) and K-VO_x-NT (b, d, f).

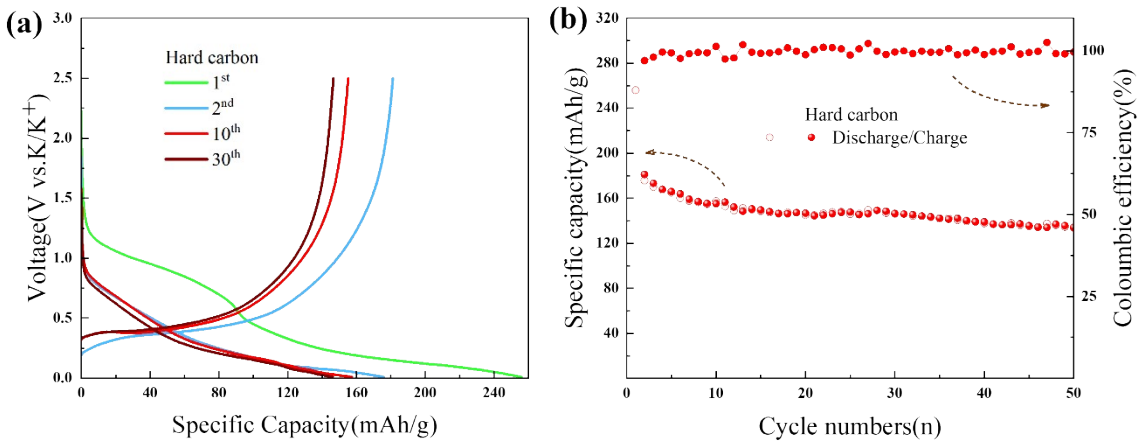

Figure S6. The 1st, 2nd, 10th and 30th GCD profiles (a) and cycling performance (b) of standard hard carbon in half-cell configuration under 50 mA g^{-1} between 0.01-2.5 V.

Fig. S6 (a) and (b) show the 1st, 2nd, 10th and 30th galvanostatic charge-discharge profiles and cycling performance of standard hard carbon in half-cell configuration. At a current density of 50 mA g^{-1} within the voltage range of 0.01–2.5 V, this hard carbon delivered an initial discharge specific capacity of 256.0 mAh g^{-1}, which decreased to 157.4, 146.2 and 133.7 mAh g^{-1} at the 10th,30th and 50th cycles, respectively.

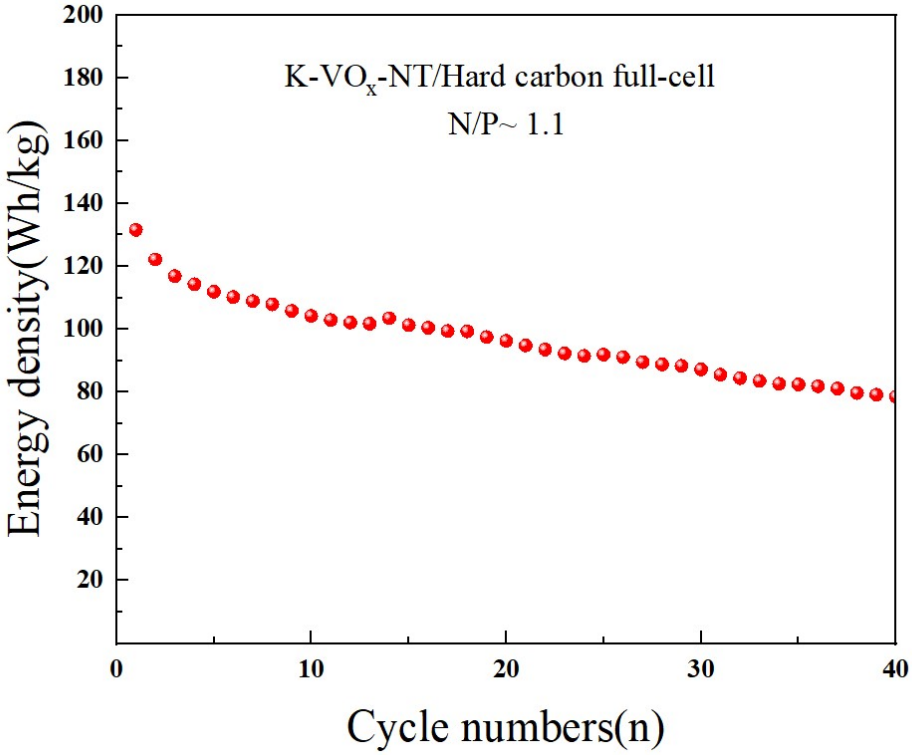

Figure S7. The evolution of energy density for K-VO_x-NT/Hard carbon full-cell in cycling process.

The energy density value is calculated based on the mass of the K-VO_x-NT cathode, without considering the mass of electrolyte and standard anode. The energy densities at the 1st, 20th, and 40th cycles are 136.0, 96.3, and 78.5 Wh kg^{-1}, respectively.

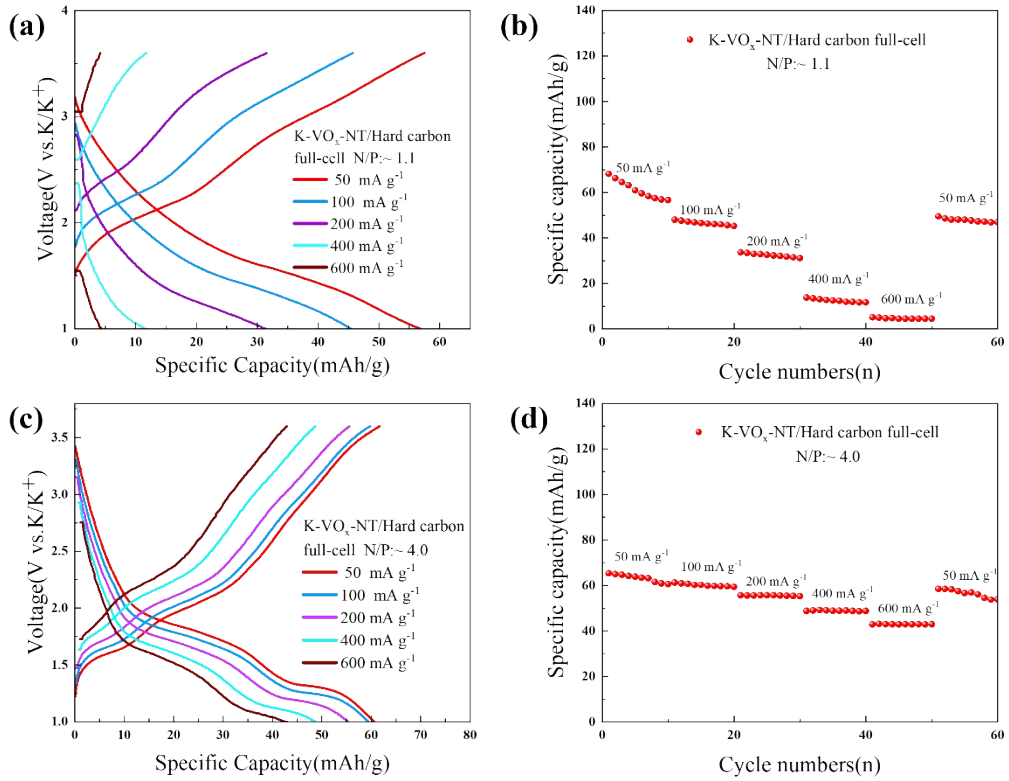

Figure S8. Typical GCD profiles (a) at 10th cycle for each rate tests and corresponding rate capability (b) of K-VO_x-NT/Hard carbon full-cell (N/P ratio: ~ 1.1) under different current densities; Typical GCD profiles (c) at 10th cycle for each rate tests and corresponding rate capability (d) of K-VO_x-NT/Hard carbon full-cell (N/P ratio: ~ 4) under different current densities.

The rate capabilities under different N/P ratios (~ 1.1 and 4.0) for K-VO_x-NT in full-cell configuration were evaluated. At the condition of ~1.1 for N/P ratio, as depicted in Fig. S8(a) and (b), the full-cell exhibits the discharge capacities of 56.7, 45.3, 31.2, 11.7, 4.5, and 47.0 mAh g^{-1} under continuously changing current densities of 50, 100, 200, 400, 600, and 50 mA g^{-1} for the 10th cycle at each rate test. In comparison, with regard to the full-cell with an N/P ratio of ~4, as shown in Fig. S8(c) and (d), the

discharge capacities are 60.6, 59.4, 55.3, 48.8, 43.0, and 53.9 mAh g^{-1} under the same current densities for the 10^{th} cycle at each rate test, respectively.

This could be due to the fact that, under the condition of ~4 for N/P ratio, the hard carbon anode is very excessive, and only a small portion of hard carbon can fully participate in the storage of K^+ during cycling. As a result, the hard carbon anode predominantly stores K^+ via capacitive behavior, which does not obviously contribute to the polarization effect of full-cell. It allows the target K-VO_x-NT cathode to demonstrate its optimal rate capability. In contrast, under the condition of ~1.1 for N/P ratio, almost all hard carbon participate in the storage of K^+, which would fully utilize its both capacitance and diffusion-controlled contributions for K^+ storage [3, 4]. In this case, the hard carbon anode will lead to obvious polarization effect of full-cell configuration, thereby affecting the rate capability of target K-VO_x-NT cathode.

References:

[1] Y. Xu, H. Dong, M. Zhou, et al. Ammonium vanadium bronze as a potassium-ion battery cathode with high rate capability and cyclability[J]. *Small Methods*, 2019, 3(8): 1800349.

[2] R. Berenguer, M.O. Guerrero-Pérez, I. Guzmán, et al. Synthesis of Vanadium Oxide Nanofibers with Variable Crystallinity and V^{5+}/V^{4+} Ratios[J]. *ACS Omega,* 2017, 2: 7739-7745.

[3] S. Alvin, H. S. Cahyadi, J. Hwang, et al. Revealing the intercalation mechanisms of lithium, sodium, and potassium in hard carbon[J]. *Adv. Energy Mater.*, 2020, 10(20):

2000283.

[4] X. Xie, S. Qi, D. Wu, et al. Porous surfur-doped hard carbon for excellent potassium storage[J]. *Chin. Chem. Lett.*, 2020, 31: 223-226.